Ab Initio Molecular Dynamics Simulation of the Amorphous Structure of Ca–Mg–Cu and Ca–Mg–Zn Alloys (Preprint).

2 AUTHORS, INCLUDING:

Oleg Senkov
UES, Inc.

267 PUBLICATIONS   **3,844** CITATIONS

Ab Initio Molecular Dynamics Simulation of the Amorphous Structure of Ca-Mg-Cu and Ca-Mg-Zn Alloys

O.N. SENKOV and Y.Q. CHENG

The atomic and electronic structures of several Ca-Mg-TM amorphous alloys (TM is Cu or Zn) have been analyzed using *ab initio* molecular dynamics simulation and neutron diffraction. Partial pair distribution functions have been produced and the pair bond distances and partial coordination numbers have been reported for these alloys. Similarities and differences in the amorphous structures of the Ca-Mg-Cu and Ca-Mg-Zn alloys have been discussed. Strong interactions between Ca-Cu, Mg-Cu and Ca-Zn atom pairs rooted from the orbital hybridization of the *s-p-d* electrons have been recognized to result in noticeable shortening of respective atom pair bond distances and pronounced chemical short range ordering near the TM atoms. Voronoi tessellation analysis has shown that the polytetrahedral-type clusters and five-coordinated atom pairs dominate in the amorphous structures, which indicates that tetrahedra and pentagonal bi-pyramids are the main building blocks in these amorphous alloys.

I. INTRODUCTION

CA-MG-BASED bulk metallic glasses (BMGs) have unique properties. They are built on two simple metals, Ca and Mg, while all other BMGs are transition-metal based alloys.[1,2] Many Ca-Mg-based alloys have very good glass forming ability (GFA), and even their ternary alloys, *e.g.*, Ca-Mg-Zn or Ca-Mg-Cu, can be made fully amorphous when they are cast in ~8 to 10 mm thick plates[3–8] or up to 15 mm diameter rods.[9,10] These glasses have very low Young's and shear moduli that are comparable with the moduli of human bones,[11–13] low density (1.6 to 2.8 g/cm^3),[1] and strong relaxation dynamics of the super-cooled liquid.[14] GFA, as well as physical and mechanical properties of metallic glasses, is believed to depend on the type of short range order (SRO) and medium range order (MRO) of alloying elements in the amorphous structure. It is therefore interesting to analyze the amorphous structure of Ca-Mg-based BMGs.

Structural analysis of metal-metal BMGs is mainly focused on transition metal glasses such as Zr-Cu,[15–18] Zr-Pt,[19] and Zr-Cu-Al.[20,21] The results indicate that the packing of atoms in these materials is not random, but is strongly influenced by chemical interactions. In particular, icosahedral SRO has been identified and correlated to their good GFA.[22] On the other hand, the atomic structure of Ca-Mg-Zn BMGs, identified with the use of X-ray and neutron diffraction and Reverse Monte Carlo

(RMC) simulation, shows no icosahedral SRO.[23] Instead, five-fold bonds in the form of pentagonal bi-pyramids have been found to be the most populous structural units in these BMGs.[23] A large fraction of five-fold bonds and the lack of icosahedral SRO has also been found in the molecular dynamic (MD) simulated amorphous structure of Mg-Cu alloys.[24]

In the present work, the atomic structures of several Ca-Mg-Cu and Ca-Mg-Zn BMGs were simulated with the use of *ab initio* (quantum) molecular dynamics (QMD) simulation. The simulated structures were then used to calculate partial (PRDF) and total (RDF) radial distribution functions, pair bond distances and partial and total coordination numbers. The QMD-simulated results were validated through the experimentally determined RDFs.

II. EXPERIMENTAL PROCEDURES

QMD simulation of the amorphous structures of the $Ca_{60}Mg_{15}Zn_{25}$, $Ca_{60}Mg_{25}Zn_{15}$, $Ca_{60}Mg_{15}Cu_{25}$, $Ca_{60}Mg_{25}Cu_{15}$, $Ca_{50}Mg_{25}Cu_{25}$, and $Ca_{40}Mg_{25}Cu_{35}$ alloys was conducted using the Vienna *ab initio* Simulation Package (VASP).[25] The Projector Augmented-Wave (PAW) method[26,27] and Perdew-Burke-Ernzerhof (PBE) functional[28,29] were used to describe interacting valence electrons. Cubic simulation boxes with periodic boundary conditions contained 200 atoms, and the box size was determined by the density of the modeled material. The simulation was conducted at Γ point only, with a first order Methfessel-Paxton smearing function (σ = 0.2 eV). The liquid was equilibrated at 1000 K (727 °C), then was quenched to 300 K (27 °C) in 100 K (100 °C) temperature steps, equilibrating at each temperature for 3000 steps. Another 3000 consecutive configurations were further sampled at 300 K (27 °C) with a time step of 5 fs, and averaged PRDFs, $g_{ij}^{QMD}(r)$, were calculated from these

O.N. SENKOV, Senior Scientist, is with the UES, Inc., Dayton, OH, and also with the Air Force Research Laboratory, Wright Patterson Air Force Base, OH 45433. Contact email: oleg.senkov@wpafb.af.mil Y.Q. CHENG, R&D Associate, is with the Chemical and Engineering Materials Division, Oak Ridge National Laboratory, Oak Ridge, TN 37831, and also with the Department of Materials Science and Engineering, Johns Hopkins University, Baltimore, MD 21218.

Table I. Density (in g/cm^3 and Atoms/Å^3) of Ca-Mg-TM (TM is Cu or Zn) Amorphous Alloys Studied in This Work

Alloy	Density	
	g/cm^3	Atoms/Å^3
Ca$_{40}$Mg$_{25}$Cu$_{35}$	2.936 ± 0.007	0.03987
Ca$_{50}$Mg$_{25}$Cu$_{25}$	2.439 ± 0.003	0.03497
Ca$_{60}$Mg$_{25}$Cu$_{15}$	2.039 ± 0.003	0.03097
Ca$_{60}$Mg$_{15}$Cu$_{25}$	2.367 ± 0.004	0.03271
Ca$_{60}$Mg$_{25}$Zn$_{15}$	2.004 ± 0.004	0.03023
Ca$_{60}$Mg$_{15}$Zn$_{25}$	2.289 ± 0.007	0.03130

configurations using Eq. [1], thus taking into account thermal vibrations and assuming no structural relaxation within 15 ps.

$$g_{ij}(r) = \frac{1}{4\pi r^2 c_j \rho_o} \frac{dn_{ij}(r)}{dr} \qquad [1]$$

Here dn_{ij} are the number of elements of type j between distances r and $r + dr$ from an element of type i, c_j is the atomic fraction of the element of type j, and ρ_o is the alloy density. The QMD models provided a complete set of six simulated PRDFs for each of the studied alloys, which well agreed with the experimental diffraction data. Due to the limited box size and the periodic boundary conditions, $g_{ij}^{QMD}(r)$ were calculated at $r \le 9$ Å.

Fully amorphous samples of the studied Ca-Mg-Cu and Ca-Mg-Zn alloys were prepared by melt-spinning in the form of ribbons as described in Reference 23. The densities, ρ_o, of the amorphous alloys were measured with a helium pycnometer AccuPyc 1330 V1.03 and the values (in g/cm^3 and atoms/Å^3) are given in Table I. Neutron diffraction experiments were conducted at room temperature under vacuum using the General Materials (GEM) diffractometer at the ISIS high-intensity pulsed neutron source (Rutherford Appleton Laboratory, Didcot, U.K.)[30] and yielded the neutron total-scattering structure factors (SSF), $S(Q)$:

$$S(Q) = \frac{1}{N}\frac{d\sigma}{d\Omega} - \sum_{i=1}^{3} c_i b_i^2 \qquad [2]$$

Here $\frac{1}{N}\frac{d\sigma}{d\Omega}$ is the differential neutron cross-section per unit solid angle Ω for the 3-component alloy, c_i and b_i are, respectively, the atomic fraction and the coherent bound neutron scattering length of element i. Each $S(Q)$ was Fourier transformed to give a real space neutron total RDF, $G(r)$, defined as[31,32]

$$G(r) = \sum_{i,j=1}^{n} c_i c_j b_i b_j [g_{ij}(r) - 1]$$

$$= \frac{1}{2\pi^2 r \rho_o} \int_0^{\infty} QS(Q)L(Q)\sin(rQ)dQ \qquad [3]$$

The Lorch modification function,[33] $L(Q)$, with a maximum momentum transfer Q_{max} of 25 Å^{-1} was used to reduce termination ripples in the Fourier transform (Eq. [3]).

Using Eq. [1], the partial coordination number of an element j in the first coordination shell of the element i was determined:

$$CN = 4\pi c_j \rho_o \int_{r_{min}}^{r_{max}} g_{ij} r^2 dr \qquad [4]$$

Here r_{min} and r_{max} are the positions of the start and end of the first peak in the respective $g_{ij}(r)$.

The simulated structures were statistically analyzed using pair and three-body correlation functions, Voronoi tessellation and nearest neighbor approaches, which allowed calculation of local structural features (SRO and MRO) such as total and partial CN, type and distribution of characteristic coordination polyhedra, atomic volume, and local packing fraction.

III. RESULTS AND DISCUSSION

A. *Structure Factors and Radial Distribution Functions*

The experimental SSFs, $S(Q)$, for the six amorphous alloys are given in Figure 1. The $S(Q)$ curves show a pronounced peak in the Q range from 2 to 3 Å^{-1} and several small diffuse peaks at higher Q values. The intensities of these peaks decrease quickly with Q and no oscillations are apparent beyond ~15 Å^{-1}. As the Cu and Zn concentrations increase, the first diffraction peak broadens (Figure 1). The presence of a pre-peak at $Q \approx 0.8$ to 1.5 Å^{-1} may indicate the presence of MRO in these alloys,[34,35] as well as the fluctuation in the atomic scattering cross-sections: the solutes, Cu, Zn and Mg, have larger neutron scattering cross-sections than the solvent, Ca.

The experimental RDFs, $G(r)$, are given in Figure 2 as solid lines. Systematic changes of the shape of the first RDF peak, which is located at $r \approx 2.1$ to 4.5 Å, with the alloy composition are observed (Figure 2). For example, the first RDF peak in Ca$_{60}$Mg$_{15}$Cu$_{25}$ has a maximum at $r = 3.05$ Å and two shoulders, one at $r = 2.58$ Å and another at $r = 3.70$ Å. As the amount of Ca decreases and the amounts of Cu and Mg increase, the intensity of the first shoulder increases and the intensity of the second shoulder decreases. On the other hand, an increase in the concentration of Mg at the expense of Cu results in the intensity of the second shoulder to exceed the intensity of the former maximum (compare RDFs of Ca$_{60}$Mg$_{15}$Cu$_{25}$ and Ca$_{60}$Mg$_{25}$Cu$_{15}$ in Figure 2). Replacing Cu with Zn noticeably decreases the intensity of the first shoulder. Because the first RDF peak is a sum of the concentration- and scattering length-weighted peaks of the six relevant PRDFs (Eq. [3]), such a strong concentration dependence of the shape of the first RDF peak is apparently due to different partial coordination numbers and pair bond distances in the studied alloys. The very different neutron scattering length of Cu ($b_{Cu} = 7.718$ fm) and Zn ($b_{Zn} = 5.680$ fm) need also to be taken into account when comparing Ca-Mg-Cu and Ca-Mg-Zn.

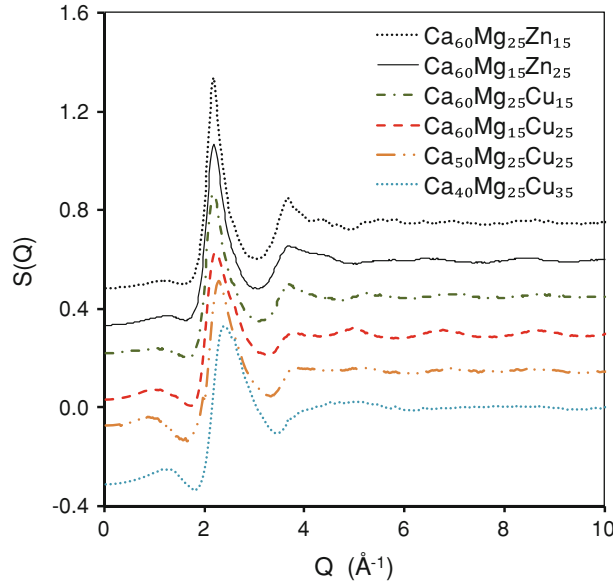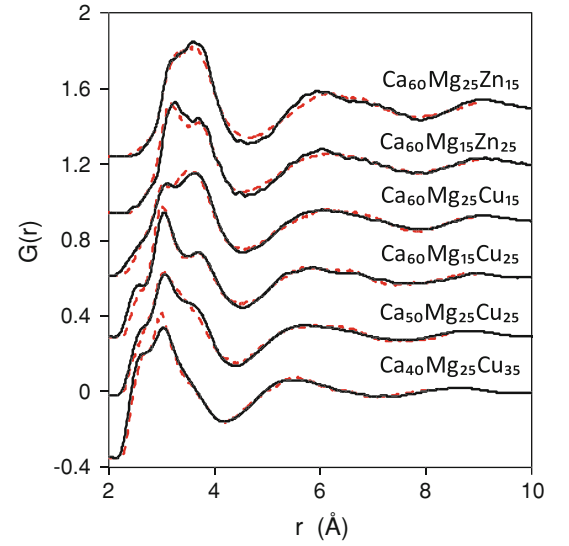Fig. 1—Total neutron scattering factors of several Ca-Mg-Zn and Ca-Mg-Cu amorphous alloys.

Fig. 2—Experimental (solid lines) and QMD-simulated (dashed lines) total radial distribution functions, $G(r)$, of Ca-Mg-Zn and Ca-Mg-Cu amorphous alloys.

Figure 3 shows six QMD-simulated PRDFs for the $Ca_{60}Mg_{15}Zn_{25}$, and $Ca_{60}Mg_{15}Cu_{25}$ amorphous alloys. The PRDFs are rather smooth since they account for atom vibrations. The first peak of each of the PRDFs corresponds to the atom pair interactions within the first coordination shell and it provides information on the nearest neighbor atom pair bond distance distributions and partial coordination numbers around the alloying elements. Comparison of the PRDFs of the $Ca_{60}Mg_{15}Zn_{25}$, and $Ca_{60}Mg_{15}Cu_{25}$ amorphous alloys shows that the intensities of the Ca-Ca, Ca-Mg and Ca-Zn peaks in the $Ca_{60}Mg_{15}Zn_{25}$ alloy are similar to the intensities of the respective Ca-Ca, Ca-Mg and Ca-Cu peaks in the $Ca_{60}Mg_{15}Cu_{25}$ alloy. At the same time the intensities of the Zn-Zn and Mg-Zn peaks are smaller and the intensity of the Mg-Mg peak is larger in $Ca_{60}Mg_{15}Zn_{25}$ than the respective intensities of the Cu-Cu, Mg-Cu and Mg-Mg peaks in $Ca_{60}Mg_{15}Cu_{25}$. This interesting observation may indicate that the Ca-Ca, Ca-Mg and Ca-Zn(Cu) interactions are similar in these alloys, while the tendencies for the Cu-Cu and Mg-Cu bonding are stronger than for the Zn-Zn and Mg-Zn bonding. Mg atoms seem to have higher tendency to cluster in the $Ca_{60}Mg_{15}Zn_{25}$ alloy than in the $Ca_{60}Mg_{15}Cu_{25}$ alloy.

Figure 4 illustrates the composition dependence of two PRDFs, $g_{Cu-Cu}(r)$ and $g_{Ca-Mg}(r)$ for the four Ca-Mg-Cu amorphous alloys. The effect of the composition on the position of the first PRDF peak is weak relative to the effect on the positions of the higher order peaks. This indicates, to the first order, that bond distances between respective atom pairs in the first coordination shell are weakly affected by the composition in the Ca-Mg-Cu system. The noticeable composition dependence in the positions of the second and higher order PRDF peaks should then indicate that the pair bond angular distributions are different in these alloys.[23] A stronger composition dependence of the intensity of

the first peak for the Cu-Cu PRDF than for the Ca-Mg PRDF may indicate that the Cu-Cu chemical order is stronger than the Ca-Mg chemical order.

Using the QMD-simulated PRDFs, $g_{ij}(r)$, known concentrations, c_i, and known neutron scattering lengths, b_i, of the alloying elements,[36] the simulated total RDFs were obtained for every alloy by utilizing Eq. [3] and compared with the respective experimental neutron RDFs (Figure 2). A very good agreement is seen. Since the QMD simulations were conducted completely independently from the neutron diffraction experiments, these excellent concords indicate that the simulated PRDFs are statistically consistent with the amorphous structures of the studied alloys and they can be used to obtain statistical information on the effect of the alloy composition on the SRO in these alloy systems.

B. *Atom Pair Bond Distances*

Using the QMD-simulated PRDFs, the most frequent (mode, r_{ij}^{Mode}), weighted average (mean, r_{ij}^{Mean}) and cut-off (maximum, $r_{ij}^{Cut-off}$) distances between atom pairs in the first coordination shell were calculated for the studied alloys and their values are given in Tables II, III, and IV, respectively. The weighted average distances, r_{ij}^{Mean}, between the i and j atoms were calculated using the following equation[23]:

$$r_{ij}^{Mean} = \int_{0}^{r_{ij}^{Cut-off}} r_{ij}g_{ij}(r)dr \Big/ \int_{0}^{r_{ij}^{Cut-off}} g_{ij}(r)dr \qquad [5]$$

The r_{Mode} values (Table II) are always smaller than the respective r_{Mean} values (Table III). This indicates that the first-shell $g_{ij}(r)$ peaks are asymmetric (non-Gaussian). The difference is larger for the Zn- than for the Cu-containing pairs, which may indicate a stronger
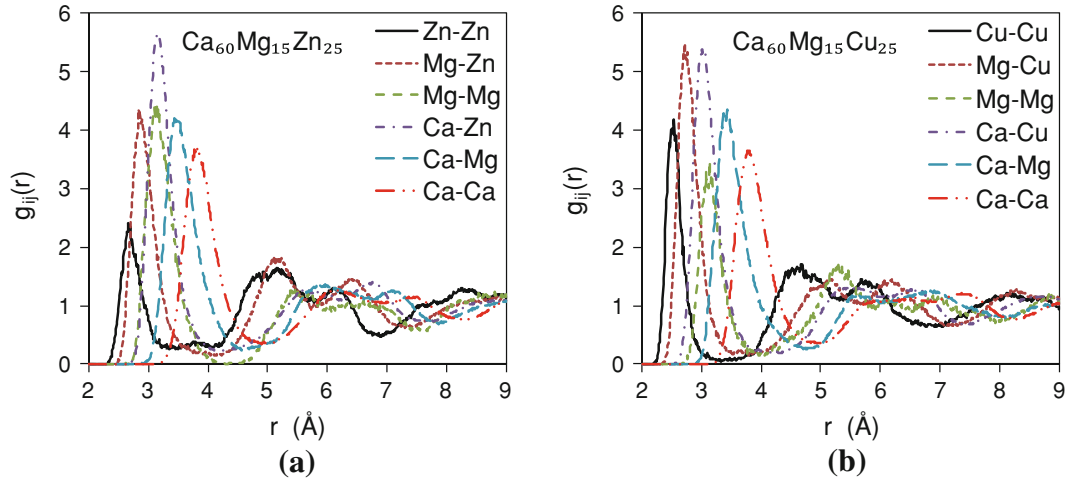
Fig. 3—QMD-simulated partial radial distribution functions, $g_{ij}(r)$, for (*a*) $Ca_{60}Mg_{15}Zn_{25}$ and (*b*) $Ca_{60}Mg_{15}Cu_{25}$ amorphous alloys.
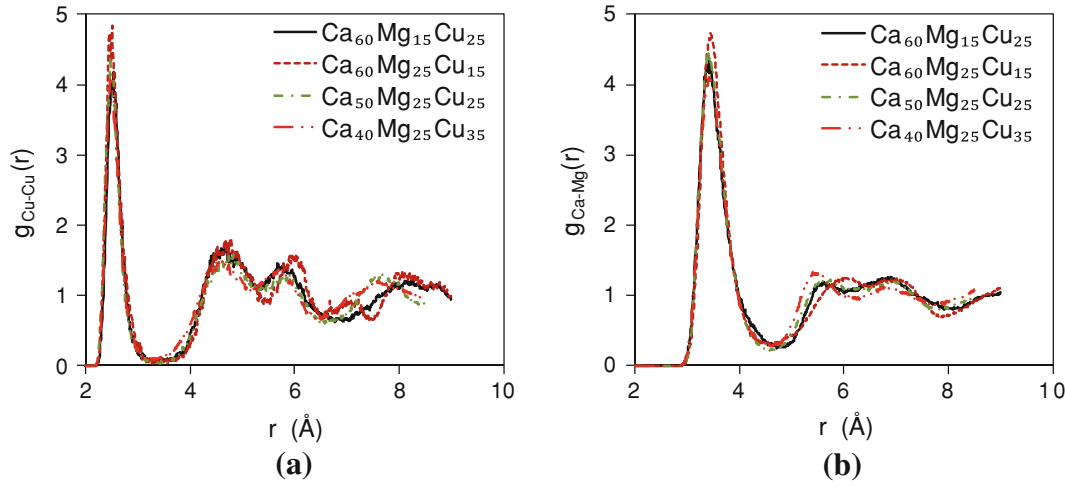

Fig. 4—Composition dependence of two PRDFs: (*a*) $g_{Cu\text{-}Cu}(r)$ and (*b*) $g_{Ca\text{-}Mg}(r)$ for Ca-Mg-Cu amorphous alloys.

interaction of Cu, than Zn, with other elements. The r_{Mode} and r_{Mean} values can be compared with atomic separations in crystalline metals and alloys. Crystalline metallic separations, r_M, and covalent distances, r_C, were estimated as a sum of metallic and covalent radii of respective elements (Table V). The metallic radii are half the nearest distance between atoms in crystal lattices of the respective pure metals.[37] The covalent atomic separations were obtained from Reference 38, based on the analysis of the nearest distances in crystalline intermetallic compounds reported in the Cambridge Structural Database. From Table V, the r_{Mean} and r_{Mode} values for Ca-Cu, Ca-Zn, and Mg-Cu atom pairs are smaller than r_M. However, for all other atomic pairs r_{Mean} values are larger and r_{Mode} values are smaller than r_M. At the same time, r_{Mode} for the atom pairs containing Cu are even smaller than the respective covalent bond distances in crystalline compounds. The Mg-Cu (2.73 Å), Ca-Cu (3.03 Å) and Ca-Zn (3.14 Å) mode pair distances are much shorter than those calculated from the Ca-Ca, Mg-Mg, Cu-Cu and Zn-Zn r_{Mode} values (*i.e.*, 2.82, 3.13, and 3.20 Å,

respectively, Table V). Shortening of Mg-Cu and Y-Cu bonds has also been observed in amorphous $Mg_{60}Cu_{30}Y_{10}$.[39] Such bond shortening often indicates strong chemical interactions between these atom pairs. No bond shortening is observed between Ca-Mg and Mg-Zn pairs.

The observation that some nearest-neighbor bond lengths are shorter than those in the competing long-range ordered crystals may help explain why these Ca-Mg-Cu and Ca-Mg-Zn alloys are easy glass formers. The equilibrium crystalline phases that compete with the amorphous phase appear to minimize total energy by sacrificing optimal SRO to achieve beneficial long-range order. On the other hand, the absence of long-range atomic order allows metallic glasses to reduce the energy difference between the metastable glass and equilibrium crystal(s) by optimizing short-range atomic interactions and arranging the atoms in efficiently packed clusters.[40–43] The largest contribution to condensed phase stability is expected to come from nearest-neighbor interactions and volume minimization, so that the optimized short-range interactions, as well as the presence of

MRO, in metallic glasses can produce structures that have only a small energetic disadvantage relative to the equilibrium crystalline structure.[22,23] Kinetic constraints from quenching and packing frustration restrict the long range atomic redistribution needed to achieve long-range order and to further minimize the total

system energy, thus favoring glass formation. The present results suggest that metallic glasses not only have SRO, but may have "better" combination of short-range topological and chemical order (in terms of optimal bond length and/or atomic arrangement) than the competing crystals.

Table II. The Most Frequent (Mode) Distances (in Angstroms) Between Pair Atoms in Ca-Mg-TM (TM = Cu or Zn) Amorphous Alloys, in Accord to QMD Simulations

Alloy	Ca-Ca	Ca-Mg	Ca-TM	Mg-Mg	Mg-TM	TM-TM
$Ca_{60}Mg_{15}Zn_{25}$	3.81	3.44	3.14	3.16	2.83	2.67
$Ca_{60}Mg_{25}Zn_{15}$	3.82	3.48	3.14	3.18	2.94	2.57
$Ca_{60}Mg_{15}Cu_{25}$	3.78	3.43	3	3.14	2.72	2.54
$Ca_{60}Mg_{25}Cu_{15}$	3.78	3.46	3.03	3.08	2.72	2.51
$Ca_{50}Mg_{25}Cu_{25}$	3.75	3.41	3.07	3.13	2.75	2.48
$Ca_{40}Mg_{25}Cu_{35}$	3.75	3.42	3.02	3.14	2.71	2.47

Table III. Weighted Average (Mean) Distances (in Angstroms) Between Pair Atoms in the First Shell in Ca-Mg-TM (TM = Cu or Zn) Amorphous Alloys, in Accord to QMD Simulations

Alloy	Ca-Ca	Ca-Mg	Ca-TM	Mg-Mg	Mg-TM	TM-TM
$Ca_{60}Mg_{15}Zn_{25}$	4.00	3.67	3.30	3.27	3.06	2.83
$Ca_{60}Mg_{25}Zn_{15}$	4.01	3.65	3.31	3.37	3.05	2.76
$Ca_{60}Mg_{15}Cu_{25}$	4.00	3.67	3.18	3.25	2.88	2.60
$Ca_{60}Mg_{25}Cu_{15}$	4.00	3.64	3.19	3.29	2.87	2.60
$Ca_{50}Mg_{25}Cu_{25}$	4.01	3.62	3.25	3.24	2.89	2.58
$Ca_{40}Mg_{25}Cu_{35}$	3.95	3.64	3.21	3.31	2.83	2.59

Table IV. The First Shell Cut-Off Distances Between Pair Atoms (in Angstroms) in Ca-Mg-TM Amorphous Alloys (TM = Cu or Zn), in Accord to QMD Simulations

Alloy	Ca-Ca	Ca-Mg	Ca-TM	Mg-Mg	Mg-TM	TM-TM
$Ca_{60}Mg_{15}Zn_{25}$	4.91	4.55	4.21	4.33	4.13	3.46
$Ca_{60}Mg_{25}Zn_{15}$	4.95	4.55	4.2	4.33	3.85	3.46
$Ca_{60}Mg_{15}Cu_{25}$	4.93	4.72	4.19	4.01	3.84	3.33
$Ca_{60}Mg_{25}Cu_{15}$	4.94	4.58	4.13	4.05	3.89	3.31
$Ca_{50}Mg_{25}Cu_{25}$	4.99	4.58	4.4	3.97	3.84	3.42
$Ca_{40}Mg_{25}Cu_{35}$	4.88	4.63	4.26	4.22	3.58	3.25

C. Coordination Numbers and Chemical Short Range Order

The average partial and total coordination numbers around Ca, Mg and TM atoms (TM is Cu or Zn), from the QMD simulations, are given in Table VI. There is almost no effect from replacing Cu with Zn on the partial and total coordination numbers around Ca and Mg atoms in the $Ca_{60}Mg_{15}TM_{25}$ and $Ca_{60}Mg_{25}TM_{15}$ amorphous alloys (the first 4 columns in Table VI). The total coordination number around Ca and Mg are $CN_{Ca} = 14.3$ and $CN_{Mg} = 11.3$ to 11.5 for $Ca_{60}Mg_{25}TM_{15}$ and $CN_{Ca} = 14.4$ and $CN_{Mg} = 11.9$ to 12.0 for $Ca_{60}Mg_{15}TM_{25}$. The number of TM and Ca increase and Mg decrease in the first coordination shell of Ca and Mg clusters with an increase in the concentration of the TM element in these alloys. At the same time, Cu has a slightly different neighbor environment than Zn. In particular, the amount of Ca is slightly lower and Mg slightly higher around Cu than around Zn. This is in agreement with the earlier discussed observation that the Mg-Cu interactions are stronger than Mg-Zn interactions.

Increasing the Cu concentration from 15 to 35 at. pct continuously increases the total coordination numbers CN_{Ca} from 14.3 to 16.2 and CN_{Mg} from 11.3 to 12.8, due to a faster increase in the number of smaller Cu atoms (CN_{Ca-Cu} and CN_{Mg-Cu} increase from 1.6 to 4.9 and from 1.1 to 3.2, respectively) and a slower decrease in the amount of the larger Ca atoms (CN_{Ca-Ca} decreases from 9.2 to 7.0 and CN_{Mg-Ca} decreases from 8.5 to 6.9) (Table VI). On the other hand, CN_{Cu} almost does not depend on the alloy composition. However, similar to the environment around Ca and Mg, CN_{Cu-Cu} increases from 0.6 to 1.6 and CN_{Cu-Ca} decreases from 6.4 to 5.6 with the increase in Cu concentration. The number of Mg atoms around Ca, Mg and Cu has a tendency to weakly increase with an increase in the concentration of Cu (Table VI).

To determine if the atoms in the amorphous structure are distributed randomly or they have a tendency to form specific clusters, the degree of chemical short range

Table V. Metallic, r_m,[37] Covalent, r_c,[38] mode, r_{Mode}, and mean, r_{Mean}, Bond Distances Between Ca, Mg and Cu(Zn) Atom Pairs

	Ca-Ca	Ca-Mg	Ca-Cu	Mg-Mg	Mg-Cu	Cu-Cu	Ca-Zn	Mg-Zn	Zn-Zn
r_M (Å)	3.94	3.57	3.25	3.20	2.88	2.56	3.31	2.94	2.68
r_C (Å)	3.52	3.17	3.08	2.82	2.73	2.64	2.98	2.63	2.44
r_{Mode} (Å)	3.78	3.44	3.03	3.14	2.73	2.50	3.14	2.89	2.62
r_{Mean} (Å)	4.00	3.65	3.21	3.29	2.87	2.59	3.31	3.06	2.80
100 pct $(r_{Mean}/r_{Mode} - 1)$	5.82	6.10	5.94	4.78	5.13	3.60	5.41	5.88	6.87
100 pct $(r_M/r_{Mode} - 1)$	4.23	3.78	7.26	1.91	5.49	2.40	5.41	1.73	2.29
100 pct $(r_C/r_{Mode} - 1)$	−6.88	−7.85	1.65	−10.19	0.00	5.60	−5.10	−9.00	−6.87
100 pct $(r_M/r_{Mean} - 1)$	−1.50	−2.19	1.25	−2.74	0.35	−1.16	0.00	−3.92	−4.29

r_m and r_c are compared to r_{Mode} and r_{Mean} from the QMD PRDFs. r_{Mode} and r_{Mean} are the average values for the studied alloys.

Table VI. Partial and Total Coordination Numbers Around Ca, Mg and TM (TM = Cu or Zn) Atoms in the Ca-Mg-Zn and Ca-Mg-Cu Amorphous Alloys, in Accord to QMD Simulations

CN	$Ca_{60}Mg_{15}Zn_{25}$	$Ca_{60}Mg_{25}Zn_{15}$	$Ca_{60}Mg_{15}Cu_{25}$	$Ca_{60}Mg_{25}Cu_{15}$	$Ca_{50}Mg_{25}Cu_{25}$	$Ca_{40}Mg_{25}Cu_{35}$
Ca-Ca	9.3	9.1	9.3	9.2	8.6	7.0
Ca-Mg	2.1	3.4	2.3	3.5	3.8	4.3
Ca-TM	3.0	1.8	2.8	1.6	3.2	4.9
Total	14.4	14.3	14.4	14.3	15.6	16.2
Mg-Ca	8.5	8.3	9.0	8.5	7.7	6.9
Mg-Mg	1.5	2.4	1.0	1.8	2.1	2.6
Mg-TM	1.9	0.8	2.0	1.1	2.1	3.2
Total	11.9	11.5	12.0	11.3	11.8	12.8
TM-Ca	7.3	7.1	6.7	6.4	6.4	5.6
TM-Mg	1.1	1.4	1.2	1.8	2.1	2.3
TM-TM	0.8	0.8	1.0	0.6	1.0	1.6
Total	9.2	9.3	8.9	8.8	9.5	9.4

Table VII. The Short-Range Order Parameters, $\alpha_{i(jk)}$, for the First Coordination Shell of Ca, Mg and TM Atoms in the Ca-Mg-TM Amorphous Alloys (TM is Cu or Zn)

$\alpha_{i(jk)}$, $i =$	Ca	Mg	TM
$Ca_{60}Mg_{15}Zn_{25}$	0.11	−0.03	−0.22
$Ca_{60}Mg_{25}Zn_{15}$	0.09	−0.06	−0.08
$Ca_{60}Mg_{15}Cu_{25}$	0.11	−0.08	−0.18
$Ca_{60}Mg_{25}Cu_{15}$	0.11	−0.13	−0.10
$Ca_{50}Mg_{25}Cu_{25}$	0.10	−0.11	−0.19
$Ca_{40}Mg_{25}Cu_{35}$	0.05	−0.05	−0.29

order (CSRO) in the first coordination shell of Ca, Mg and TM atoms was estimated using a CSRO parameter, $\alpha_{i(jk)}$, which was defined for ternary alloys in Reference[44]:

$$\alpha_{i(jk)} = 1 - \left(CN_{ij} + CN_{ik}\right)/\left((c_j + c_k)CN_i\right) \quad \text{for } i \neq j \neq k \tag{6}$$

Here c_j is the atomic fraction of the element j, CN_{ij} is the partial coordination number of element j in the first coordination shell of the element i, and CN_i is the total coordination number of element i. Negative $\alpha_{i(jk)}$ values indicate the presence of CSRO, *i.e.*, the total concentration of j and k atoms in the first coordination shell exceed their total average concentration in the alloy. The positive values indicate the excess of i-elements in the first coordination shell of i atom, *i.e.*, chemical short range clustering (CSRC) of atoms i.

The $\alpha_{i(jk)}$ values for the studied Ca-Mg-TM glasses are given in Table VII. The parameter $\alpha_{i(jk)}$ is positive for Ca atoms and is negative for Mg and TM atoms. This result indicates that Ca atoms tend to cluster with each other, while Mg and TM atoms have a tendency to attract unlike atoms in the first coordination shell and form CSRO. This tendency for CSRO is stronger for the TM elements than for Mg in all studied alloys, except $Ca_{60}Mg_{25}Cu_{15}$. The CSRO of the TM element with Ca and Mg increases with an increase in the concentration of the TM element in the alloy. The presence of CSRO

near TM and Mg and CSRC near Ca atoms indicates that the amorphous structure of the Ca-Mg-TM alloys is not a random solution of the alloying elements, but it consists of TM- and Mg-centered atomic clusters, with specific CSROs. Stronger CSRO around the TM elements may indicate that the TM-centered clusters dominate over the Mg-centered clusters.

D. *Voronoi Analysis of the Atomic Clusters in Ca-Mg-TM Amorphous Alloys*

Voronoi tessellation and the resulting Voronoi cells allow identification of characteristic coordination polyhedra present in an amorphous structure.[23,42] A coordination polyhedron is defined as an i-centered cluster with vertices at the first-shell atom positions and edges coinciding with the interatomic bonds in the first shell.[45] Each coordination polyhedron can be assigned a Voronoi signature (n_3, n_4, n_5, n_6), where n_m is the number of vertices common to m polyhedron faces (or edges).[46] m is also called the vertex coordination. Those i-centered clusters with the same Voronoi signature are considered to be topologically equivalent (even though they may not be identical).

Table VIII lists Ca, Mg and TM-centered clusters identified in the amorphous structures of the studied Ca-Mg-TM alloys. Only clusters, which are present at a fraction, f_P, of 0.1 or higher in at least one of the alloys are tabulated. Just three types of the Ca-centered polyhedra have the fractions $f_P \geq 0.1$. These are (0,2,8,4), (0,1,10,4) and (0,2,8,5). The total fraction of these clusters varies from 0.36 in $Ca_{60}Mg_{25}Zn_{15}$ to 0.075 in $Ca_{40}Mg_{25}Cu_{35}$ and many other different types of Ca-centered polyhedra are present at $f_P \sim 0.05$ or less. Many different types of clusters, with low fraction of each of the type, may indicate that the Ca-centered clusters are not likely building blocks for the amorphous structures.

Six characteristic Mg-centered and five TM-centered clusters with $f_P \geq 0.1$ are also shown in Table VIII. All of them except (1,3,3,3) are Kasper-type polyhedra,[45] which account for 36 to 80 pct among the Mg-centered clusters and 44 to 82 pct among the Cu-centered clusters (these clusters are the least populated in $Ca_{40}Mg_{25}Cu_{35}$ and most populated in $Ca_{60}Mg_{15}Zn_{25}$). The high fraction

Table VIII. Fraction of Clusters Identified in the Amorphous Structures of Ca-Mg-TM Alloys

Cluster type	$Ca_{60}Mg_{15}Zn_{25}$	$Ca_{60}Mg_{25}Zn_{15}$	$Ca_{60}Mg_{15}Cu_{25}$	$Ca_{60}Mg_{25}Cu_{15}$	$Ca_{50}Mg_{25}Cu_{25}$	$Ca_{40}Mg_{25}Cu_{35}$
Ca-centered clusters						
(0,2,8,4)	0.12	0.15	0.08	0.10	0.05	0.01
(0,1,10,4)	0.04	0.11	0.18	0.11	0.07	0.04
(0,2,8,5)	0.04	0.10	0.06	0.04	0.10	0.03
Mg-centered clusters						
(0,2,8,1)	0.23	0.10	0.13	0.16	0.06	0.00
(0,3,6,3)	0.10	0.04	0.13	0.10	0.02	0.00
(0,0,12,0)	0.20	0.14	0.07	0.04	0.06	0.08
(0,2,8,2)	0.10	0.18	0.03	0.10	0.10	0.02
(0,3,6,4)	0.07	0.16	0.17	0.00	0.16	0.06
(0,1,10,2)	0.10	0.06	0.03	0.08	0.04	0.20
TM-centered clusters						
(0,3,6,0)	0.30	0.13	0.24	0.27	0.16	0.11
(1,3,3,3)	0.08	0.00	0.10	0.02	0.06	0.07
(0,3,6,1)	0.20	0.10	0.14	0.10	0.10	0.04
(0,2,8,0)	0.16	0.27	0.12	0.03	0.12	0.11
(0,2,8,1)	0.08	0.20	0.06	0.03	0.04	0.10

Only clusters populated with the fractions of 0.1 or higher in *at least one of the alloys* are tabulated.

Table IX. Global and Atomic Packing Fractions in Ca-Mg-TM Amorphous Alloys

Alloy	Packing Fraction	Average Voronoi Volume ($\mathring{A}^3$)			Atomic Packing Fraction		
		Ca	Mg	TM	Ca	Mg	TM
$Ca_{60}Mg_{15}Zn_{25}$	0.76	41.0	24.2	14.3	0.78	0.71	0.71
$Ca_{60}Mg_{25}Zn_{15}$	0.76	40.6	25.3	15.9	0.79	0.68	0.64
$Ca_{60}Mg_{15}Cu_{25}$	0.78	39.9	23.7	12.4	0.80	0.72	0.71
$Ca_{60}Mg_{25}Cu_{15}$	0.77	40.5	24.2	12.8	0.79	0.71	0.68
$Ca_{50}Mg_{25}Cu_{25}$	0.79	38.8	24.1	12.6	0.83	0.71	0.70
$Ca_{40}Mg_{25}Cu_{35}$	0.80	38.0	22.6	12.0	0.84	0.76	0.73

of the selected TM- and Mg-centered Kasper-type polyhedra should indicate that the amorphous structure of the Ca-Mg-TM alloys mainly consists of these clusters, which is in agreement with the recently proposed ECP model of the amorphous structure.[43,47] Since Kasper polyhedra are polytetrahedral, and many other polyhedra also contain tetrahedra, we conclude that the topological SRO of Ca-Mg-TM is polytetrahedral in nature, which has been demonstrated in many other metallic glasses.[22] The current study therefore further supports the idea that the SRO of MGs is characterized by polytetrahedral packing *via* Kasper polyhedra and their distorted variants.

The analysis of the most populated clusters given in Table VIII indicates that five-coordinated vertices dominate in all the clusters; however, the amorphous structures of the Ca-Mg-TM glasses contain a low fraction of icosahedral SRO (Kasper polyhedra with (0,0,12,0) Voronoi index). This is presumably due to the large mismatch of atomic sizes in the nearest neighbor shell (*e.g.*, r_{Ca} = 1.97 Å and r_{Cu} = 1.28 Å), which renders the distorted Kasper polyhedra more topologically favored. A large fraction of five-fold bonds and the lack of icosahedral SRO have also been found in the MD-simulated amorphous structure of Mg-Cu alloys.[24] The dominance of five-fold vertices

suggests that tetrahedra prefer to cluster into pentagonal bi-pyramids.

Table VIII also demonstrates the different local topology in $Ca_{60}Mg_{15}Zn_{25}$ and $Ca_{60}Mg_{15}Cu_{25}$ (columns 1 and 3), which differs by only the type of the TM element. Specifically, because Cu is smaller in size, and has obvious bond shortening with both Ca and Mg, it is expected to induce higher CN around Ca/Mg, as well as more distortion in the Kasper polyhedra. Indeed, the most popular cluster type around Ca is (0,1,10,4) with CN = 15 in $Ca_{60}Mg_{15}Cu_{25}$, and (0,2,8,4) with CN = 14 in $Ca_{60}Mg_{15}Zn_{25}$. For Mg centered clusters, it is (0,3,6,4) with CN = 13 in $Ca_{60}Mg_{15}Cu_{25}$, and (0,2,8,1) with CN = 11 and (0,0,12,0) with CN = 12 in $Ca_{60}Mg_{15}Zn_{25}$.

E. Local Volume and Packing Fraction

Assuming atoms are hard spheres, the global packing fraction can be easily calculated using the atomic radii and the density of the alloy. This approach yields a packing fraction of 0.76 to 0.80 for the alloys in this study (Table IX). However, this treatment is very crude, and it does not provide information on local packing fraction specific to an atom, an element, or a cluster. In the following we propose a method that can be used to describe the local volume and packing fraction.

Table X. Cluster Packing Fractions in Ca-Mg-TM Amorphous Alloys

Alloy	Average Vertex Coordination			Average Cluster Volume (Å^3)			Cluster Packing Fraction		
	Ca	Mg	TM	Ca	Mg	TM	Ca	Mg	TM
$Ca_{60}Mg_{15}Zn_{25}$	5.13	4.97	4.78	107.6	83.3	64.0	0.77	0.75	0.76
$Ca_{60}Mg_{25}Zn_{15}$	5.14	5.00	4.84	108.5	84.0	65.1	0.77	0.74	0.74
$Ca_{60}Mg_{15}Cu_{25}$	5.14	5.00	4.77	104.2	81.9	57.9	0.79	0.77	0.77
$Ca_{60}Mg_{25}Cu_{15}$	5.12	4.96	4.77	107.7	82.0	58.7	0.78	0.76	0.76
$Ca_{50}Mg_{25}Cu_{25}$	5.17	5.02	4.80	103.7	77.6	58.4	0.80	0.77	0.78
$Ca_{40}Mg_{25}Cu_{35}$	5.16	5.04	4.86	96.9	73.6	53.4	0.82	0.80	0.80

The weighted Voronoi tessellation assigns each atom with a Voronoi cell, and its volume can be considered as the atomic volume (*i.e.*, the volume occupied by the center atom at its position). The summation of the atomic volume defined as such equals to the total volume of the alloy. Therefore, the ratio between the hard sphere volume (calculated from the metallic radius) and the atomic volume (Voronoi cell volume) is on average smaller than 1, and reflects the packing density around the specific atom (*i.e.*, atomic packing fraction in Table IX). The challenge now is how to define the packing fraction for a short-range cluster, and the key is to find out a way to quantify the actual volume occupied by a cluster in the amorphous matrix. An *i*-centered cluster consists of the atom *i* in the center and $CN_i = \sum_{j=1}^{3} CN_{ij}$ atoms in the first shell. The atoms in the first shell are shared with other neighbor clusters. The average volume of the cluster, V_i, is then defined as:

$$V_i = v_i + \sum_{j=1}^{3} \frac{CN_{ij} v_j}{1 + K_{ij}} \qquad [7]$$

Here v_i and v_j are the average Voronoi volumes of atoms *i* and *j*, and K_{ij} is the average number of clusters, which are the neighbors to the *i*-centered cluster and which share the atom *j* in their first shell. The averaging is conducted over the whole number of clusters of type *i* presented in the amorphous structure and vertices of type *j* in the cluster *i*. It is expected that $K_{ij} = 1 + \mu_{ij}$, where μ_{ij} is the average coordination of vertex *j* in the *i*-centered cluster:

$$\mu_{ij} = \sum_{m=3}^{6} m_{ij} f_{m_{ij}} \qquad [8]$$

and thus

$$V_i = v_i + \sum_{j=1}^{3} \frac{CN_{ij} v_j}{2 + \mu_{ij}} \qquad [9]$$

Here $f_{m_{ij}}$ is the fraction of *j* vertices with the vertex coordination m_{ij} in all *i*-centered clusters. Indeed, in general two neighbor clusters can share a face, an edge, or a vertex. The average number of faces or edges, which have a common vertex *j* is equal, by definition, to μ_{ij}. A geometric analysis shows that the neighbor clusters having a common vertex *j*, can fill space only if they share *j*-vertex-containing faces with the *i*-centered cluster and thus the number of these neighbors should be equal to μ_{ij}. One additional neighbor cluster will share only the vertex *j* with the *i*-centered cluster. The μ_{ij} values can be directly obtained from the results of the Voronoi tessellation of the amorphous structure.

Equations [8] and [9] were used to calculate the average vertex coordinations and average volumes of the Ca-, Mg- and TM-centered clusters for all the studied alloys. The results are given in Table X. The average coordination of the Ca-, Mg-, and TM-vertices is ~5.1, 5.0, and 4.8, respectively, and it weakly depends on the alloy composition. At the same time, the average cluster volumes are noticeably composition-dependent. As it is expected from the numbers and radii of the atoms in the clusters, the Ca-centered clusters have the largest volume (~97 to 109 Å^3) and the TM-centered clusters have the smallest volume (~53 to 64 Å^3). The Mg-centered clusters have an intermediate volume of ~74 to 84 Å^3. The cluster volumes in the Zn-containing alloys are larger than in the respective Cu-containing alloys, probably because the atomic radius of Zn is larger than that of Cu, and Cu incurs more significant bond shortening. In the Ca-Mg-Cu alloys, the volume of the clusters decreases with an increase in the concentration of Cu and/or decrease in the concentration of Ca/Mg due to an increasing number of Cu and decreasing number of Ca/Mg in the first shell of all three type clusters.

The average packing fraction of the *i*-type clusters was estimated by calculating the total volume of the atoms belonging to the averaged *i*-cluster (using the equation similar to Eq. [9], where the Voronoi volumes are replaced with respective atom volumes) and dividing it by V_i^{aver}. Atomic radii reported in Table V were used to calculate the atom volumes. The results are given in Table X. The Ca-centered clusters are packed slightly more densely than the Mg- and Cu-centered clusters. In Ca-Mg-Zn alloys, the average packing fraction of Ca-centered clusters is ~0.77 and it decreases to ~0.74 to 0.75 for Mg-centered and to ~0.74 to 0.76 for Zn-centered clusters. The packing fraction of the clusters is slightly smaller in the Zn-containing alloys than in the respective Cu-containing alloys, probably due to stronger interactions of Cu with other elements leading to more intense bond shortening. An increase in the concentration of Cu in the Ca-Mg-Cu alloys increases the clusters' packing fraction, thus supporting the presence of strong Cu-Cu, Cu-Mg and Cu-Ca bonding in these amorphous alloys.
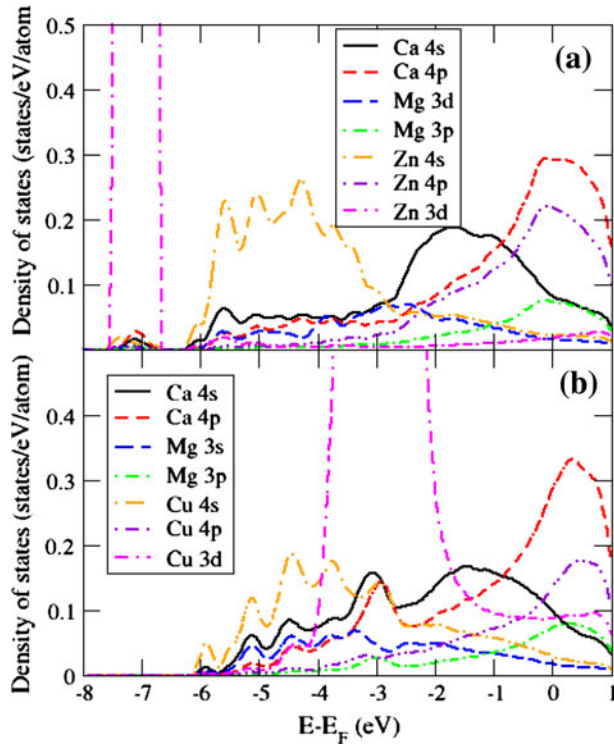
Fig. 5—Site- and orbital-projected electronic DOS for (*a*) Ca$_{60}$Mg$_{15}$Zn$_{25}$ and (*b*) Ca$_{60}$Mg$_{15}$Cu$_{25}$ amorphous alloys.

The cluster volume and packing fraction data do not appear to be systematically correlated with the GFA of these alloys. This is not surprising because, in addition to the uncertainties in determining the volume at atomic level, the many factors that can influence the GFA, including the relative stability of the competing crystalline phases and the interfacial energy, often make it difficult to establish a simple method to predict the ability of an alloy to form glass.

F. *Electronic Structure of Ca-Mg-TM Amorphous Alloys*

It has been shown in the above discussion that the presence of Cu or Zn in the Ca-Mg-TM amorphous alloys leads to different bonding characters and thus properties. It is therefore intriguing to examine the electronic structure of Ca-Mg-Cu and Ca-Mg-Zn, especially the differences associated with the TM element. To this end, site- and orbital-projected electronic density of states (DOS) was calculated using the configurations obtained in QMD simulation, on a $3 \times 3 \times 3$ Monkhorst-Pack grid. Only valence electrons (2 for Ca, 2 for Mg, 11 for Cu, and 12 for Zn) are accounted for as the low-lying core electrons are unlikely to participate in the bonding. Wigner radii for the decomposition are 1.947 Å for Ca, 1.524 Å for Mg, 1.270 Å for Zn, and 1.312 Å for Cu. The results are compared in Figure 5.

The most prominent difference between Figure 5(a) (Ca$_{60}$Mg$_{15}$Zn$_{25}$) and Figure 5(b) (Ca$_{60}$Mg$_{15}$Cu$_{25}$) is the very different position of the narrow and intense

3d-band: for Zn it is over 7 eV below the Fermi level, while for Cu it is 2 to 3 eV below the Fermi level. As a result, the 3d-band of Zn barely overlaps with the *s*- and *p*-conduction/bonding bands in Ca/Mg, whereas for Cu the overlap is significant. Such overlap between the 3d-band of TM and the sp-band of simple metals is known to result in strong chemical interactions and orbital hybridization, as previously demonstrated in Al-Cu, where the Al-Cu bonds are shortened by over 6 pct.[20] The DOS in Figure 5 may explain why Cu induces more obvious bond shortening than Zn (*e.g.*, Ca-Cu bond is shortened by 7.26 pct, while Ca-Zn bond is shortened by only 5.41 pct).

IV. CONCLUSIONS

1. The atomic structures of six Ca-Mg-TM ternary metallic glasses (TM is Cu or Zn) have been analyzed using neutron diffraction and *ab initio* molecular dynamics (QMD) modeling. All six partial radial distribution functions (PRDFs), $g_{ij}(r)$, have been identified for each alloy.
2. The nearest-neighbor mode bond lengths are shorter than those in competing crystals. A noticeable shortening of Ca-Cu, Mg-Cu, and Ca-Zn bond distances indicate strong interactions between these atom pairs, as supported by the calculated electronic structure. It is suggested that the bond shortening is enabled by the absence of long-range atomic order, which lowers the free energy of metallic glasses and increases GFA.
3. Pronounced CSRO near TM atoms, chemical short range clustering (CSRC) near Ca atoms and a neutral environment near Mg atoms are shown. Increasing the Cu concentration from 15 to 35 atomic percent increases the total coordination number around Ca, CN$_{Ca}$, from 13.6 to 15.0, while CN$_{Mg}$ and CN$_{Cu}$ remain unchanged at $\approx$12.5 and $\approx$10.4, respectively. The partial coordination numbers depend on alloy composition, so that the number of Ca atoms decreases, the number of Cu atoms increases and the number of Mg atoms is almost constant with increasing TM concentration.
4. Voronoi tessellation show that many types of coordination polyhedra are present, but the most common are Kasper and distorted Kasper polyhedra at the favorable CNs. The fractions and distributions of these clusters depend on alloy composition. Polytetrahedral-type clusters and five-coordinated vertices dominate in the amorphous structures, which indicates that tetrahedra and pentagonal bi-pyramids are the main building blocks in these amorphous alloys.

REFERENCES

1. O.N. Senkov, D.B. Miracle, V. Keppens, and P.K. Liaw: *Metall. Mater. Trans. A*, 2008, vol. 39A, pp. 1888–1900.
2. A. Takeuchi and A. Inoue: *Mater. Trans. JIM*, 2005, vol. 46, pp. 2817–29.
3. O.N. Senkov and J.M. Scott: *Scripta Mater.*, 2004, vol. 50, pp. 449–52.
4. O.N. Senkov and J.M. Scott: *Mater. Lett.*, 2004, vol. 58, pp. 1375–78.
5. O.N. Senkov and J.M. Scott: *J. Non-Cryst. Solids*, 2005, vol. 351, pp. 3087–94.
6. O.N. Senkov, J.M. Scott, and D.B. Miracle: *Mater. Trans.*, 2007, vol. 48, pp. 1610–16.
7. O.N. Senkov, J.M. Scott, and D.B. Miracle: *J. Alloy. Compd.*, 2006, vol. 424, pp. 394–99.
8. O.N. Senkov, D.B. Miracle, and J.M. Scott: *Intermetallics*, 2006, vol. 14, pp. 1055–60.
9. E.S. Park and D.H. Kim: *J. Mater. Res.*, 2004, vol. 19, pp. 685–88.
10. E.S. Park, W.T. Kim, and D.H. Kim: *Mater. Sci. Forum*, 2005, vols. 475–479, pp. 3415–18.
11. V. Keppens, Z. Zhang, O.N. Senkov, and D.B. Miracle: *Philos. Mag.*, 2007, vol. 87, pp. 503–08.
12. D. Okai, M. Inoue, T. Mori, T. Fukami, T. Yamasaki, H.M. Kimura, and A. Inoue: *J. Alloy. Compd.*, 2010, vol. 504S, pp. S95–S97.
13. Z. Zhang, V. Keppens, O.N. Senkov, and D.B. Miracle: *Mater. Sci. Eng. A*, 2007, vol. 471, pp. 151–54.
14. O.N. Senkov and D.B. Miracle: *Metall. Mater. Trans. A*, 2010, vol. 41A, pp. 1677–84.
15. N. Mattern, A. Schöps, U. Kühn, J. Acker, O. Khvostikova, and J. Eckert: *J. Non-Cryst. Solids*, 2008, vol. 354, pp. 1054–60.
16. D. Ma, A.D. Stoica, X.L. Wang, Z.P. Lu, M. Xu, and M. Kramer: *Phys. Rev. B*, 2009, vol. 80, p. 014202.
17. Y.Q. Cheng, H.W. Sheng, and E. Ma: *Phys. Rev. B*, 2008, vol. 78, p. 014207.
18. Y.Q. Cheng, A.J. Cao, H.W. Sheng, and E. Ma: *Acta Mater.*, 2008, vol. 56, pp. 5263–75.
19. N.A. Mauro, V. Wessels, J.C. Bendert, S. Klein, A.K. Gangopadhyay, M.J. Kramer, S.G. Hao, G.E. Rustan, A. Kreyssig, A.I. Goldman, and K.F. Kelton: *Phys. Rev. B*, 2011, vol. 83, pp. 184109/1–8.
20. Y.Q. Cheng, E. Ma, and H.W. Sheng: *Phys. Rev. Lett.*, 2009, vol. 102, p. 245501.
21. K. Georgarakis, A.R. Yavari, D.V. Louzguine-Luzgin, J. Antonowicz, M. Stoica, Y. Li, M. Satta, A. LeMoulec, G. Vaughan, and A. Inoue: *Appl. Phys. Lett.*, 2009, vol. 94, p. 191912.
22. Y.Q. Cheng and E. Ma: *Prog. Mater. Sci.*, 2011, vol. 56, pp. 379–473.
23. O.N. Senkov, D.B. Miracle, E.R. Barney, A.C. Hannon, Y.Q. Cheng, and E. Ma: *Phys. Rev. B*, 2010, vol. 82, p. 104206.
24. N.P. Bailey, J. Schiotz, and K.W. Jacobsen: *Phys. Rev. B*, 2004, vol. 69, p. 144205.
25. G. Kresse and J. Hafner: *Phys. Rev. B*, 1993, vol. 47, pp. 558–61.
26. P.E. Blochl: *Phys. Rev. B*, 1994, vol. 50, pp. 17953–77.
27. G. Kresse and D. Joubert: *Phys. Rev. B*, 1999, vol. 59, pp. 1758–75.
28. J.P. Perdew, K. Burke, and M. Ernzerhof: *Phys. Rev. Lett.*, 1996, vol. 77, pp. 3865–69.
29. J.P. Perdew, K. Burke, and M. Ernzerhof: *Phys. Rev. Lett.*, 1997, vol. 78, p. 1396.
30. A.C. Hannon: *Nucl. Instrum. Methods Phys. Res. A*, 2005, vol. 551, pp. 88–107.
31. T.E. Faber and J.M. Ziman: *Philos. Mag.*, 1965, vol. 11, pp. 153–73.
32. D.A. Keen: *J. Appl. Crystallogr.*, 2001, vol. 34, pp. 172–77.
33. E. Lorch: *J. Phys. C*, 1969, vol. 2, p. 229.
34. L. Zhang, Y. Wu, X. Bian, H. Li, W. Wang, and S. Wu: *J. Non-Cryst. Solids*, 2000, vol. 262, pp. 169–76.
35. N.A. Mauro, W. Fu, J.C. Bendert, Y.Q. Cheng, E. Ma, and K.F. Kelton: *J. Chem. Phys.*, 2012, vol. 137, pp. 044501/1–10.
36. V.F. Sears: *Neutron News*, 1992, vol. 3 (3), pp. 29–37.
37. N.N. Greenwood and A. Earnshaw: *Chemistry of the Elements*, 2nd ed., Butterworth-Heinemann, Oxford, U.K., 1997.
38. B. Cordero, V. Gómez, A.E. Platero-Prats, M. Revés, J. Echeverría, E. Cremades, F. Barragán, and S. Alvarez: *Dalton Trans.*, 2008, vol. 21, pp. 2832–38.
39. P. Jovari, K. Saksl, N. Pryds, B. Lebech, N.P. Bailey, A. Mellergård, R.G. Delaplane, and H. Franz: *Phys. Rev. B*, 2007, vol. 76, p. 054208.
40. D.B. Miracle, W.S. Sanders, and O.N. Senkov: *Philos. Mag.*, 2004, vol. 83, p. 2409.
41. D.B. Miracle, O.N. Senkov, W.S. Sanders, and K.L. Kendig: *Mater. Sci. Eng. A*, 2004, vol. 3750377, pp. 150–56.
42. R. Zallen: *The Physics of Amorphous Solids*, Wiley-VCH, Weinheim, 2004.
43. D.B. Miracle: *Nat. Mater.*, 2004, vol. 3, pp. 697–702.
44. O.N. Senkov, Y.Q. Cheng, D.B. Miracle, E.R. Barney, A.C. Hannon, and C.F. Woodward: *J. Appl. Phys.*, 2012, vol. 111, p. 123515.
45. F.C. Frank and J.S. Kasper: *Acta Crystallogr.*, 1958, vol. 11, pp. 184–90.
46. J.L. Finney: *Proc. R. Soc. A*, 1970, vol. 319, pp. 495–507.
47. D.B. Miracle: *Acta Mater.*, 2006, vol. 54, pp. 4317–36.